Title	In-beam γ-ray spectroscopy of ^{34,36,38}Mg : Merging the N=20 and N=28 shell quenching
Author(s)	Doornenbal, P.; Scheit, H.; Takeuchi, S. et al.
Citation	Physical Review Letters. 2013, 111(21), p. 212502-212502
Version Type	VoR
URL	https://hdl.handle.net/11094/51206
rights	© 2013 American Physical Society
Note	

The University of Osaka Institutional Knowledge Archive : OUKA

https://ir.library.osaka-u.ac.jp/

The University of Osaka

In-Beam γ-Ray Spectroscopy of ^{34,36,38}Mg: Merging the $N = 20$ and $N = 28$ Shell Quenching

P. Doornenbal,[1,*] H. Scheit,[1,2] S. Takeuchi (武内 聡),[1] N. Aoi (青井考),[1] K. Li (李闊昂),[1,2]
M. Matsushita (松下昌史),[1,3] D. Steppenbeck,[1] H. Wang (王赫),[1,2] H. Baba (馬場秀忠),[1] H. Crawford,[4] C. R. Hoffman,[5]
R. Hughes,[6] E. Ideguchi (井手口栄治),[7] N. Kobayashi (小林信之),[8] Y. Kondo (近藤洋介),[8] J. Lee (李曉菁),[1]
S. Michimasa (道正新一郎),[7] T. Motobayashi (本林透),[1] H. Sakurai (櫻井博儀),[1] M. Takechi (武智麻耶),[1]
Y. Togano (栂野泰宏),[1] R. Winkler,[9] and K. Yoneda (米田健一郎)[1]

[1]*RIKEN Nishina Center, Wako, Saitama 351-0198, Japan*
[2]*Peking University, Beijing 100871, People's Republic of China*
[3]*Department of Physics, Rikkyo University, Toshima, Tokyo 172-8501, Japan*
[4]*Lawrence Berkeley National Laboratory, Berkeley, California 94720, USA*
[5]*Physics Division, Argonne National Laboratory, Argonne, Illinois 60439, USA*
[6]*Department of Physics, University of Richmond, Richmond, Virginia 23173, USA*
[7]*Center for Nuclear Study, University of Tokyo, RIKEN Campus, Wako, Saitama 351-0198, Japan*
[8]*Department of Physics, Tokyo Institute of Technology, Meguro, Tokyo 152-8551, Japan*
[9]*National Superconducting Cyclotron Laboratory, Michigan State University, East Lansing, Michigan 48824, USA*

Neutron-rich $N = 22, 24, 26$ magnesium isotopes were studied via in-beam γ-ray spectroscopy at the RIKEN Radioactive Isotope Beam Factory following secondary fragmentation reactions on a carbon target at ≈ 200 MeV/nucleon. In the one- and two-proton removal channels from ^{39}Al and ^{40}Si beams, two distinct γ-ray transitions were observed in ^{38}Mg, while in the one-proton removal reaction from ^{37}Al a new transition was observed in addition to the known $2_1^+ \rightarrow 0_{\text{g.s.}}^+$ decay. From the experimental systematics and comparison to theoretical predictions it is concluded that the transitions belong to the $2_1^+ \rightarrow 0_{\text{g.s.}}^+$ and $4_1^+ \rightarrow 2_1^+$ decays in ^{36}Mg and ^{38}Mg, respectively. For ^{34}Mg, previously reported 2_1^+ and 4_1^+ level energies were remeasured. The deduced $E(4_1^+)/E(2_1^+)$ ratios for ^{34,36,38}Mg of 3.14(5), 3.07(5), and 3.07(5) are almost identical and suggest the emergence of a large area of deformation extending from the $N = 20$ to the $N = 28$ shell quenching.

The structure of atomic nuclei across the Segré chart is subject to a plethora of transformations. In the conventional image, regions of spherical and deformed nuclei alternate within this chart according to a constant set of proton and neutron numbers. These "magic" numbers, which were first correctly reproduced by Jensen and Mayer [1,2] for nuclei lying close to the valley of stability, mark the nuclear shell closures for which spherical shapes are anticipated. In contrast, nuclei located between the lines of the grid of magic numbers are expected to become increasingly deformed towards midshell regions. Initially, the set of magic numbers was considered invariant across the Segré chart. However, scientific progress in the past decades showed that for systems with an unbalanced proton-to-neutron ratio, the original magic numbers may disappear while others emerge. At present, notable experimental and theoretical research is dedicated to a better understanding of the driving forces behind the nuclear shell evolution (see, e.g., [3]).

Neutron-rich $_{10}$Ne, $_{11}$Na, and $_{12}$Mg isotopes are located within a region known as the "island of inversion" [4] and form one of the most notable regions of sudden shell structure change. In groundbreaking studies by Klapisch and Thibault [5,6], abnormally high masses for ^{31,32}Na were

discovered, leading to the presumption that the $\nu f_{7/2}$ orbitals intrude into the sd shell orbitals, thereby quenching the $N = 20$ shell gap [7]. Later theoretical works predicted, however, that not the entire orbitals are inverted but $\nu(sd)^{-2}(fp)^2(2\hbar\omega)$ configurations are lowered so much in energy that they form the ground states for $10 \le Z \le 12$, $20 \le N \le 22$ nuclei instead [4,8]. Another example of shell evolution is given by the disappearance of the $N = 28$ magic number originally formed by the large $\nu f_{5/2}$-$\nu f_{7/2}$ spin-orbit splitting. Here, the removal of only a few protons from $^{48}_{20}$Ca leads to a $N = 28$ shell gap reduction in $^{46}_{18}$Ar [9], $^{44}_{16}$S exhibits collective characteristics [10], and a large deformation arises for $^{42}_{14}$Si [11,12].

Initially believed to be two isolated regions, we show in this Letter that the $N = 20, 28$ shell quenching is interlinked via the neutron-rich magnesium isotopes, thereby forming a new connected large area of deformation in the Segré chart. Key information on the shape of a nucleus can be obtained for even-even nuclei from the energy of the first excited 2^+ state $E(2_1^+)$, the first 4^+ state $E(4_1^+)$, and their $E(4_1^+)/E(2_1^+)$ ratio, $R_{4/2}$. Previous studies of the neutron-rich magnesium isotopes include the measurements of $E(2_1^+)$ and $R_{4/2}$ for ^{34}Mg [13] and $E(2_1^+)$ for ^{36}Mg [14]. For ^{34}Mg, a low 2_1^+ excitation energy of 660(7) keV

was observed alongside a tentative assignment of the 4_1^+ state to 2120(22) keV. This corresponds to $R_{4/2} = 3.21(5)$, close to 3.33 for a deformed rigid rotor and a vast increase from the ratio of 2.62 observed for the transitional nucleus ^{32}Mg [15], whereas a ratio of 2 represents a vibrational excitation for spherical nuclei. Similarly, the low excitation energy of 660(6) keV for the 2_1^+ state in ^{36}Mg, in combination with the observed cross sections to the ground and first excited state following two-proton knockout reactions, was explained by large intruder admixtures [14]. These findings suggest that the "island of inversion" stretches at least to neutron number $N = 24$ for the magnesium isotopes and thus beyond its originally proposed boundaries. In the present study, the experimental knowledge of $E(2_1^+)$ and $E(4_1^+)$ is extended to the $N = 26$ nucleus ^{38}Mg.

The experiment was carried out at the Radioactive Isotope Beam Factory, operated by the RIKEN Nishina Center and the Center for Nuclear Study of the University of Tokyo. A primary beam of ^{48}Ca with an average intensity of 70 particle nA and an energy of 345 MeV/nucleon was impinged on a 15 mm thick rotating Be target located at the BigRIPS radioactive isotope projectile-fragment separator's entrance [16]. From the reaction products, secondary beams were selected and purified via the $B\rho$-ΔE-$B\rho$ method, and identified with the ΔE-$B\rho$-TOF method, as described in earlier experiments [17,18].

Two secondary beam settings were applied on BigRIPS. The first focused on ^{39}Al and ^{40}Si isotopes in order to observe the $1p$ and $2p$ knockout reactions towards ^{38}Mg. The second setting was set to ^{37}Al and ^{36}Mg for knockout reactions towards ^{34,36}Mg. The rates for ^{39}Al and ^{40}Si isotopes transported through BigRIPS in the first setting were 75 and 3000 particles/sec, respectively, the second setting contained 90 particles/sec of ^{36}Mg and 400 particles/sec of ^{37}Al.

The secondary beams were incident on a 2.54 g/cm^2 thick carbon secondary target. The energies for ^{39}Al and ^{40}Si were 219 and 226 MeV/nucleon in front of the secondary target and 236 and 247 MeV/nucleon for ^{36}Mg and ^{37}Al, respectively. To detect γ rays from excited states in ^{34,36,38}Mg, the secondary target was surrounded by the DALI2 spectrometer [19], consisting of 186 large-volume NaI(Tl) crystals. The energy resolution and the efficiency were 10% (FWHM) and 20% for 1 MeV γ rays, respectively.

Reaction residues from the secondary target were identified by the ZeroDegree spectrometer [16]. Similarly, the ΔE-$B\rho$-TOF method was employed by measuring the TOF with two scintillators placed at the ZeroDegree spectrometer's first and final focal point, the position at the dispersive focus, and the energy loss with an ionization chamber at the final focal point. Unambiguous separation in charge Q and for the mass to charge ratio A/Q was provided by the ZeroDegree spectrometer, as shown in Fig. 1 for the first setting.
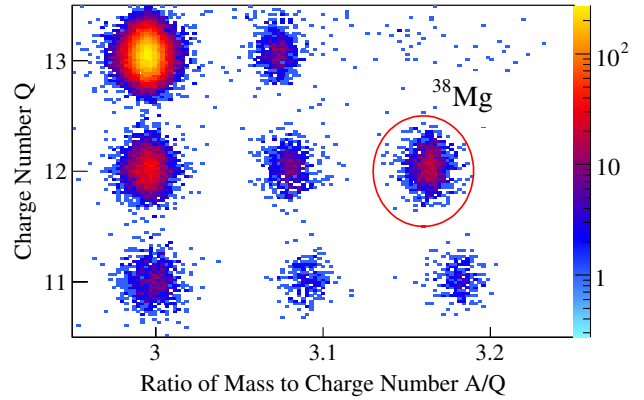

FIG. 1 (color online). Particle identification with the ZeroDegree beam line detectors behind the secondary target for ^{39}Al and ^{40}Si secondary beams. The ^{38}Mg fragments are clearly separated from other reaction products.

Two γ-ray transitions were observed in ^{38}Mg from the $1p$ and $2p$ knockout channels after correcting for the Doppler shift, as shown in Fig. 2. The energies of the two transitions, which we attribute to the $2_1^+ \rightarrow 0_{g.s.}^+$ and the $4_1^+ \rightarrow 2_1^+$ decays based on arguments presented later, were determined to be 656(6) keV and 1360(20) keV in the summed spectrum of both reaction channels. To enhance the peak-to-background ratio, the summed spectrum was restricted to γ-ray multiplicities $M_\gamma \leq 3$ in coincidence with the knockout reactions. As shown in the insets of Fig. 2, analyzing all γ-ray multiplicities failed to bring out the $4_1^+ \rightarrow 2_1^+$ transition. It is also visible that the $2p$ removal channel features more background, which might originate from more populated levels that could not be resolved and/or target excitation.
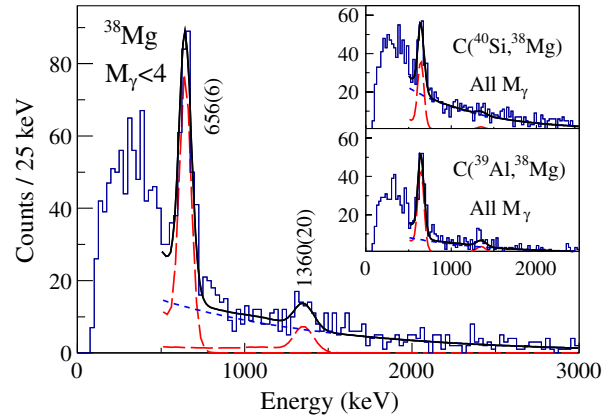

FIG. 2 (color online). Doppler corrected γ-ray energy spectra in coincidence with ^{38}Mg following $1p$- and $2p$-removal reactions. A condition for γ-ray multiplicity ($M_\gamma < 4$) was applied. The insets show the two removal channels separately for all multiplicities. We show lines containing simulated response functions at the respective observed transition energies (red long dashed line), fitted background (blue short dashed line), and their sum (black solid line).

For the transition energy determination, statistical and systematic errors were taken into account. The latter originated from the energy calibration (0.5%) and unknown lifetimes of the excited states, in particular for the first excited state, resulting in β-value and position uncertainties for the Doppler correction, as described in Refs. [17,20]. Line shape simulations were performed with GEANT4 [21] to confirm the observed γ-ray transitions. The experimental spectra were fitted with the resulting DALI2 response functions using the peak intensities and two exponentials for the background as free parameters. The fit results are overlaid on the presented experimental spectra.

The Doppler-corrected γ-ray spectra of ^{34,36}Mg are displayed in Fig. 3. For ^{36}Mg, the $2_1^+ \rightarrow 0_{g.s.}^+$ transition was observed at 662(6) keV, in agreement with the previously reported value [14]. In addition, a second γ-ray decay was seen at 1370(20) keV, which we assign to the $4_1^+ \rightarrow 2_1^+$ transition. For ^{34}Mg, transitions were observed at 652(6), 1395(15), 2480(30), and 3130(30) keV, respectively. In the earlier $2p$-knockout measurement to ^{34}Mg, γ-ray transitions

were observed at 660(10) and 1460(20) keV and assigned to the $2_1^+ \rightarrow 0_{g.s.}^+$ and $4_1^+ \rightarrow 2_1^+$ transitions [13]. While the former transition agrees well with our result, we assign the $4_1^+ \rightarrow 2_1^+$ transition to be at 1395(15) keV, which is 65 keV lower. The discrepancy may originate from the low statistics and limited mass resolution in the previous work.

A gate set on the 652(6) keV line, presented in the inset of the lower panel of Fig. 3, shows that the 1395(15) and the 2480(30) keV transitions are in coincidence with the $2_1^+ \rightarrow 0_{g.s.}^+$ decay. As no indication for the 3130(30) keV transition was found and the sum of the 652(6) and the 2480(30) keV transitions matches well in energy, it is concluded that a level at 3130(30) keV decays to the 2_1^+ and to the ground state. All observed $2_1^+ \rightarrow 0_{g.s.}^+$ and $4_1^+ \rightarrow 2_1^+$ transitions are summarized in Table I.

No direct evidence for definite spin assignments was obtained from the experiment. However, previous knock-out experiments in this region revealed that the 2_1^+ and 4_1^+ states for neutron-rich neon, magnesium, and silicon isotopes are most prevalently populated [12,13,22,23]. Further evidence for spin assignment can be based on experimental systematics and comparison to theoretical predictions. Figure 4 displays, in the top panel, the known experimental $E(2_1^+)$ and $E(4_1^+)$ excitation energies of neutron-rich silicon and magnesium isotopes as a function of the neutron number. At $N = 20$, the $E(2_1^+)$ of ^{34}Si of 3.33 MeV reflects the closed neutron shell in combination with a $Z = 14$ subshell closure. With increasing neutron number, the $E(2_1^+)$ gradually decrease until the lowest value is reached at $N = 28$ [11], thus showing no evidence for a large shell gap. In contrast, the low $E(2_1^+)$ of ^{32}Mg of 885 keV illustrates the $N = 20$ shell quenching and the heavier magnesium isotopes show remarkably little variation in their structure. A measurement of the $Z = 10$ neon isotope ^{32}Ne found an $E(2_1^+)$ at 722(9) keV and thus a slow rise in excitation energy for the $N = 22$ isotones [17], thereby establishing the magnesium excitation energies as the lowest in this region of the Segré chart. Similarly, while the $E(4_1^+)$ energies in the silicon isotopes feature some staggering, adding two and even four neutrons to ^{34}Mg does not affect the respective $E(4_1^+)$ excitation energies.
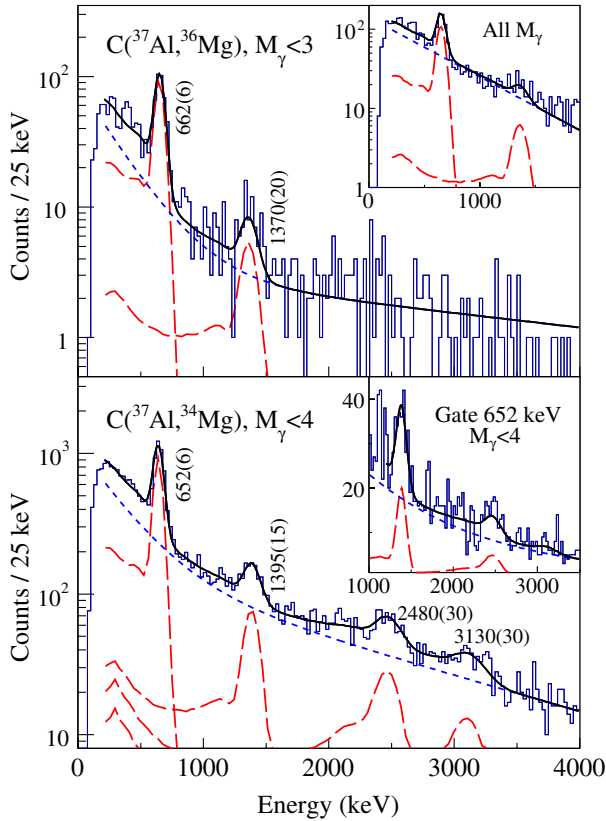

FIG. 3 (color online). Doppler corrected γ-ray energy spectra in coincidence with ^{34,36}Mg following $1p$ (upper panel) and $1p$-$2n$ removal (lower panel) reactions from the ^{37}Al secondary beam. Conditions on the maximum, coincident γ-ray multiplicity M_γ were applied. The inset of the upper panel shows the spectrum of ^{36}Mg without this condition. A gate on the 652(6) keV line was applied in the inset of the lower panel for γ-γ coincident events of ^{34}Mg.

TABLE I. Summary of observed $2_1^+ \rightarrow 0_{g.s.}^+$ and $4_1^+ \rightarrow 2_1^+$ transitions for the isotopes ^{34,36,38}Mg. For ^{34,36}Mg, previous results from Refs. [13,14] are shown for comparison.

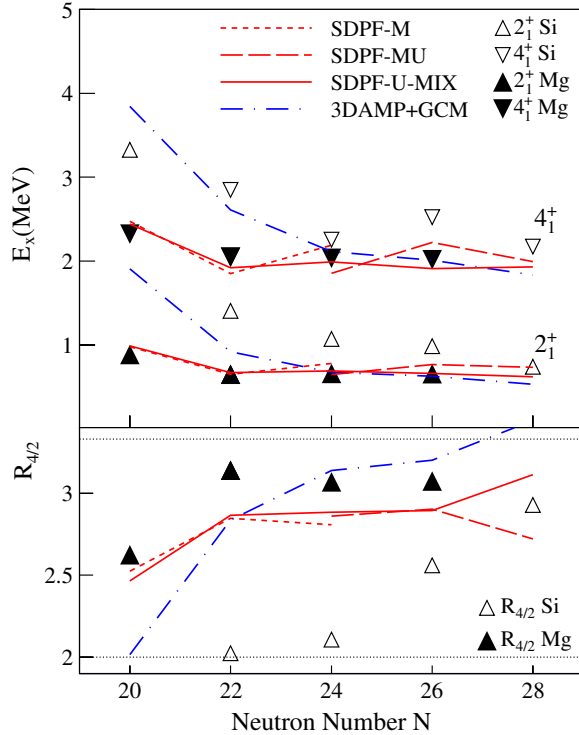|	Transition	Energy (keV)	
Isotope	$J_i^\pi \rightarrow J_f^\pi$	This work	Refs. [13,14]
^{34}Mg	$(2_1^+) \rightarrow 0_{g.s.}^+$	652(6)	660(10)
	$(4_2^+) \rightarrow (2_1^+)$	1395(15)	1460(20)
^{36}Mg	$(2_1^+) \rightarrow 0_{g.s.}^+$	662(6)	660(6)
	$(4_2^+) \rightarrow (2_1^+)$	1370(20)	
^{38}Mg	$(2_1^+) \rightarrow 0_{g.s.}^+$	656(6)	
	$(4_2^+) \rightarrow (2_1^+)$	1360(20)	

FIG. 4 (color online). The top panel displays the known experimental $E(2_1^+)$ and $E(4_1^+)$ energies for silicon (open triangles) and magnesium (filled triangles) isotopes between $N = 20$ and $N = 28$ deduced in this and earlier works [11–15,24,35,36]. In the bottom panel, the respective $R_{4/2}$ ratios are shown. The horizontal dashed lines represent the vibrational and rotational limits. The experimental findings for the magnesium isotopes are compared to shell model predictions using the SDPF-M [25] (red short dashed line), the SDPF-MU [31] (red long dashed line), the SDPF-U-MIX [26,32] (red solid line) effective interactions, and the relativistic 3DAMP + GCM model [27] (blue dash dotted line).

It is very instructive to point out the different evolution of deformation from $N = 20$ to $N = 28$ for the magnesium and silicon isotopes. For the silicon isotopes, the recently deduced $R_{4/2}$ ratios up to $N = 28$ [12,24] show a gradual increase from the vibrational limit with values around 2 at $N = 22$, 24 to the deformed ^{42}Si with $R_{4/2} = 2.93(5)$ at $N = 28$. From the observed transition energies in this work, almost constant $R_{4/2}$ ratios of 3.14(5), 3.07(5), and 3.07(5) were obtained for ^{34,36,38}Mg at $N = 22$, 24, 26, close to the ideal rigid rotor ratio value of 3.33 and increasing from $R_{4/2} = 2.62$ for the transitional nucleus ^{32}Mg. The $R_{4/2}$ for the magnesium and silicon isotopes are presented in the lower part of Fig. 4, illustrating the two different patterns towards increased deformation and accordingly shell evolution from $N = 20$ to $N = 28$.

Several predictions for 2_1^+ and 4_1^+ level energies of neutron rich magnesium isotopes have been made in the past based on the shell model (SM) [25,26] and mean field approaches [27–30]. Results from SM calculations with the SDPF-M [25], the SDPF-MU [31], and the SDPF-U-MIX [26,32] interactions and a mean field approach based on the generator coordinate method with three-dimensional angular-momentum projected wave functions (3DAMP + GCM) [27] are compared in Fig. 4 with the experimental values.

The SM calculations performed with the SDPF-M interaction provide mixing of the sd and pf shells and therefore an adequate base for studies around the "island of inversion." Excellent agreement with the experimental data is obtained for the 2_1^+ and 4_1^+ states from $N = 20$ to $N = 24$. Maximum deviations are in the order of ≈ 200 keV for the 4_1^+ states, thus supporting the spin assignments in ^{34,36}Mg. Also, the trend of increasing $R_{4/2}$ ratios is well reproduced. The values for $N = 22$, 24 fall slightly short, however, given the large ratio and small $E(2_1^+)$, correspond to a shift of only a few tens of keV for the first excited state.

To get a common description of all nuclei around the $N = 20$ and $N = 28$ shell quenching, the SDPF-U interaction [33] has been updated to SDPF-U-MIX to allow for np-nh excitations across the $N = 20$ shell gap. Predictions using this interaction provide a compelling agreement with our data for ^{34,36,38}Mg and for ^{32}Mg, again supporting our spin assignments. The downward shift from $N = 20$ to $N = 22$ for the $E(2_1^+)$ and $E(4_1^+)$ and the invariance for larger neutron numbers matches the experimental findings as well as the $R_{4/2}$ increase to ≈ 2.9. As before, a lower value for the latter corresponds to a shift of only a few tens of keV in the $E(2_1^+)$.

Also the recent SDPF-MU interaction, which highlights the role of the tensor force when approaching $N = 28$, is in good agreement with our results for ^{36,38}Mg. Here, calculations were performed without sd neutron excitations across the $N = 20$ shell, as calculations using the SDPF-M interaction suggest a diminishing intruder contribution beyond $N = 22$ (see Fig. 8 of Ref. [31]). A similar trend is observed with SDPF-U-MIX, for which average additional numbers of neutrons in the pf shell with respect to normal filling of 2.4, 1.7, and 0.5 are obtained for ^{34,36,38}Mg, respectively. Hence, the constant $E(2_1^+)$ and $E(4_1^+)$ energies in the magnesium isotopes may be caused by the interplay between a gradually decreasing influence from the $N = 20$ quenching and an increasing importance of the $N = 28$ quenching.

Beyond the present results, SDPF-MU and SDPF-U-MIX predict a well-deformed ^{40}Mg at $N = 28$. This notion is supported by the mean field calculations using the 3DAMP + GCM approach, which are unable to reproduce the $N = 20$ shell quenching for ^{32}Mg but predict large prolate deformations in the ground state and $R_{4/2} \approx 3$ for $^{34–40}$Mg. Proceeding even further, a persistent $N = 32$ (sub-)shell closure is expected from the SDPF-U-MIX interaction [26,32]. Thus, a new large-area, common subshell comprising the $0d_{3/2}$, $0f_{7/2}$, and $1p_{3/2}$ orbitals may be formed at the neutron drip-line.

In summary, we have reported on new excited states in ^{34,36,38}Mg following $1p$, $2p$, and $1p2n$ removal reactions at energies above 200 MeV/nucleon. For ^{36}Mg, a newly observed decay was assigned to the $4_1^+ \rightarrow 2_1^+$ transition, and for ^{38}Mg the two new decays were attributed to the $2_1^+ \rightarrow 0_{g.s.}^+$ and $4_1^+ \rightarrow 2_1^+$ transitions, respectively. The observed $R_{4/2}$ ratios suggest strongly deformed shapes in all neutron-rich magnesium isotopes. Our findings are supported by mean field as well as shell model calculations. Together with the data for the neutron-rich silicon isotopes, theory and experiment converge towards a persistently large deformation for the recently observed $N = 28$ magnesium isotope at the neutron drip-line [34].

    *pieter@ribf.riken.jp

[1] O. Haxel, J. Jensen, and H. Suess, Phys. Rev. **75**, 1766 (1949).

[2] M. Goeppert Mayer, Phys. Rev. **75**, 1969 (1949).

[3] O. Sorlin and M.-G. Porque, Prog. Part. Nucl. Phys. **61**, 602 (2008).

[4] E. K. Warburton, J. A. Becker, and B. A. Brown, Phys. Rev. C **41**, 1147 (1990).

[5] R. Klapisch, C. Thibault-Philippe, C. Détraz, J. Chaumont, R. Bernas, and E. Beck, Phys. Rev. Lett. **23**, 652 (1969).

[6] C. Thibault, R. Klapisch, C. Rigaud, A. Poskanzer, R. Prieels, L. Lessard, and W. Reisdorf, Phys. Rev. C **12**, 644 (1975).

[7] X. Campi, H. Flocard, A. Kerman, and S. Koonin, Nucl. Phys. **A251**, 193 (1975).

[8] A. Poves and J. Retamosa, Phys. Lett. B **184**, 311 (1987).

[9] L. Gaudefroy et al., Phys. Rev. Lett. **97**, 092501 (2006).

[10] T. Glasmacher et al., Phys. Lett. B **395**, 163 (1997).

[11] B. Bastin et al., Phys. Rev. Lett. **99**, 022503 (2007).

[12] S. Takeuchi et al., Phys. Rev. Lett. **109**, 182501 (2012).

[13] K. Yoneda et al., Phys. Lett. B **499**, 233 (2001).

[14] A. Gade et al., Phys. Rev. Lett. **99**, 072502 (2007).

[15] S. Takeuchi et al., Phys. Rev. C **79**, 054319 (2009).

[16] T. Kubo et al., Prog. Theor. Exp. Phys. **2012**, 03C003 (2012).

[17] P. Doornenbal et al., Phys. Rev. Lett. **103**, 032501 (2009).

[18] N. Kobayashi et al., Phys. Rev. C **86**, 054604 (2012).

[19] S. Takeuchi, T. Motobayashi, H. Murakami, K. Demichi, and H. Hasegawa, in *RIKEN Accelerator Progress Report* (RIKEN, Wako, 2003), Vol. 36, p. 148.

[20] P. Doornenbal et al., Nucl. Instrum. Methods Phys. Res., Sect. A **613**, 218 (2010).

[21] S. Agostinelli et al., Nucl. Instrum. Methods Phys. Res., Sect. A **506**, 250 (2003).

[22] D. Bazin et al., Phys. Rev. Lett. **91**, 012501 (2003).

[23] P. Fallon et al., Phys. Rev. C **81**, 041302 (2010).

[24] X. Liang et al., Phys. Rev. C **74**, 014311 (2006).

[25] Y. Utsuno, T. Otsuka, T. Mizusaki, and M. Honma, Phys. Rev. C **60**, 054315 (1999).

[26] A. Poves, E. Caurier, F. Nowacki, and K. Sieja, Phys. Scr. **T150**, 014030 (2012).

[27] J. M. Yao, H. Mei, H. Chen, J. Meng, P. Ring, and D. Vretenar, Phys. Rev. C **83**, 014308 (2011).

[28] T. Siiskonen, P. O. Lipas, and J. Rikovska, Phys. Rev. C **60**, 034312 (1999).

[29] M. Yamagami and Y. R. Shimizu, Phys. Rev. C **77**, 064319 (2008).

[30] K. Yoshida, Eur. Phys. J. A **42**, 583 (2009).

[31] Y. Utsuno, T. Otsuka, B. A. Brown, M. Honma, T. Mizusaki, and N. Shimizu, Phys. Rev. C **86**, 051301 (2012).

[32] E. Caurier, F. Nowacki, and A. Poves, arXiv:1309.6955.

[33] F. Nowacki and A. Poves, Phys. Rev. C **79**, 014310 (2009).

[34] T. Baumann et al., Nature (London) **449**, 1022 (2007).

[35] S. Raman, C. W. N. Jr., and P. Tikkanen, At. Data Nucl. Data Tables **78**, 1 (2001).

[36] C. Campbell et al., Phys. Rev. Lett. **97**, 112501 (2006).